

Enabling the bulk photovoltaic effect in centrosymmetric materials through an external electric field

Guilherme J. Inacio,^{1,2,*} Juan José Esteve-Paredes,³ Maurício F. C. Martins Quintela,^{2,4} Wendel S. Paz,¹ and Juan José Palacios^{2,4,5}

¹Departamento de Física, Universidade Federal do Espírito Santo, 29075-910 Vitória-ES, Brazil

²Departamento de Física de la Materia Condensada,

Universidad Autónoma de Madrid, E-28049 Madrid, Spain

³Centro de Física de Materiales, Universidad del País Vasco (UPV/EHU), E-20018 Donostia-San Sebastián, Spain

⁴Condensed Matter Physics Center (IFIMAC), Universidad Autónoma de Madrid, E-28049 Madrid, Spain

⁵Instituto Nicolás Cabrera (INC), Universidad Autónoma de Madrid, E-28049 Madrid, Spain

(Dated: December 4, 2025)

We develop a practical approach to electrically tuning the nonlinear photoresponse of two-dimensional semiconductors by explicitly incorporating a static out-of-plane electric field into the electronic ground state prior to optical excitation, as a gate bias. The method is implemented by dressing a Wannier-interpolated Hamiltonian with the field through its position matrix elements, which allows the gate bias to modify orbital hybridization and band dispersion beyond perturbative treatments. Within the independent-particle approximation, the resulting second-order (shift) conductivity is evaluated for both centrosymmetric and non-centrosymmetric layered systems. Applied to MoS₂, the approach captures the emergence of a finite shift current in centrosymmetric bilayers and the tunability of intrinsic responses in polar structures. The shift conductivity rises linearly at small fields and saturates at higher intensities, reflecting the competition between the growing shift vector and the weakening interband coupling as resonant transitions move away from high-symmetry valleys. A Taylor expansion of the field-dressed conductivity connects this behavior to the third-order optical response, revealing a unified picture of field-induced nonlinearities. These results establish field dressing of Wannier Hamiltonians as a practical route to model and predict nonlinear photocurrents in layered materials.

I. INTRODUCTION

The photoresponse of two-dimensional (2D) crystals has attracted sustained interest since the first demonstrations of efficient photodetection in graphene and transition-metal dichalcogenides (TMDs) [1–4]. Applications span integrated photonics, photovoltaics, and ultrasensitive photodetectors [5–8]. More recently, attention has shifted toward nonlinear second-order phenomena, most notably second-harmonic generation (SHG) and the bulk photovoltaic effect (BPVE), which rely on the absence of inversion symmetry [9–17]. This has motivated different strategies to activate second-order responses in nominally centrosymmetric 2D materials, including controlled strain [18–21], stacking engineering and twist angles [22–24], and out-of-plane electric fields [25, 26]. However, while electrically tunable SHG, including electric-field-induced second-harmonic (EFISH) responses where a static field activates an effective $\chi^{(2)} \propto \chi^{(3)} E_{DC}$, has been widely studied [17, 26–29], the corresponding field-induced BPVE remains comparatively unexplored.

A first step in this direction was taken by Zheng *et al.* [25], who investigated field-induced shift and injection currents in AA'- and AB-stacked bilayer graphene using a four-band π -orbital tight-binding model [17, 30, 31]. Their results showed that breaking inversion symmetry

via a perpendicular gate indeed generates finite dc photocurrents. Yet two limitations complicate the interpretation. First, pristine AA stacking is a semimetal, thus the applied field simultaneously open a gap and break inversion, making it difficult to separate symmetry effects from semimetal-to-semiconductor transitions. Second, the model couples the static field only to diagonal on-site terms, neglecting field-induced modifications of interlayer and extended hoppings. These off-diagonal contributions become important once the field hybridizes electronic states across layers, and their omission can mask or distort the true field-induced symmetry breaking.

A complementary viewpoint was provided by Fregoso and co-workers, who developed a third-order perturbative formalism in which one of the driving fields carries zero frequency [32, 33]. In this approach, the dc photocurrent in a crystal under static field is encoded in the mixed third-order tensor $\sigma_{abcd}^{(3)}(0; \omega, -\omega, 0)$, from which field-induced shift, injection, and jerk currents can be obtained. This framework is formally elegant and captures the leading linear-in-field response. However, because the static field enters only perturbatively, it cannot describe band-gap renormalization [34, 35], field-induced hybridization of Bloch states [36–38], or the eventual saturation and non-monotonic evolution of $\sigma^{(2)}$ at experimentally reasonable field strengths [39–47]. Moreover, only a single field-linear value of the effective $\sigma^{(2)}$ is obtained, leaving the full evolution from the perturbative to the strong-field regime inaccessible.

* guijanone@gmail.com, corresponding author

In this work, we demonstrate that a gate bias, applied as a static out-of-plane electric field, can induce and continuously tune shift-current responses in layered materials, including centrosymmetric bilayer crystals such as 2H MoS₂. Our approach incorporates the field directly through matrix elements of the position operator in a Wannier-interpolated Hamiltonian. Here, intersite (off-diagonal) dipole matrix elements arise naturally [48–51], allowing the field to modify not only the local potential but also orbital hybridization and electronic dispersion. This enables a fully non-perturbative treatment in the static field, capturing the onset, evolution, and eventual saturation of the shift conductivity. The method applies equally to centrosymmetric (2H) and non-centrosymmetric (3R) bilayers, as well as to monolayers with finite thickness along z . By expanding $\sigma^{(2)}(\omega; E_{\text{DC}}^z)$ in powers of the field, we recover analytically the mixed third-order tensor $\sigma_{abcd}^{(3)}(0; \omega, -\omega, 0)$ obtained in Fregoso *et al.*'s work [32, 33], establishing a direct connection between our non-perturbative field dressing and the perturbative third-order formalism. This provides a unified description of weak- and strong-field regimes and clarifies the origin of saturation at large field.

Section II introduces the formalism, including the implementation of the static field in the Wannier basis, highlighting the important role of off-diagonal position-matrix elements not present in minimal tight-binding models. It also treats the evaluation of the shift current, and its connection to third-order response theory. Section III focuses on MoS₂, where we analyze the monolayer, the centrosymmetric AA' (2H) bilayer, and the non-centrosymmetric AB (3R) bilayer, showing how the magnitude and tensor structure of the second-order response evolve under static field. Computational parameters and Wannierization details are provided in Appendix A.

II. THEORY

A. Hamiltonian with static field

Following the length-gauge formulation of Aversa-Sipe and Sipe-Shkrebttii [52, 53], previously applied in related contexts [54, 55], we consider a two-dimensional crystal whose principal axes lie in the xy plane. A static out-of-plane field $\mathbf{E}_{\text{DC}} = (0, 0, E_z)$ breaks inversion symmetry, while an in-plane monochromatic probe field $E_a^{(\text{ac})} e^{i\omega t}$ ($a = x, y$) excites the system. In the length gauge, the total Hamiltonian reads

$$\hat{H} = \hat{H}_0 - eE_{\text{DC}}\hat{r}_z - eE_a^{(\text{ac})}e^{i\omega t}\hat{r}_a, \quad (1)$$

where \hat{H}_0 is the mean-field equilibrium Hamiltonian and \hat{r} is the position operator. To treat the static field non-

perturbatively, we define

$$\hat{H}_0^{(\text{DC})} = \hat{H}_0 - eE_{\text{DC}}\hat{r}_z, \quad (2)$$

$$\hat{H}' = -eE_a^{(\text{ac})}e^{i\omega t}\hat{r}_a, \quad (3)$$

and regard \hat{H}' as a first-order optical perturbation.

It is instructive to inspect the matrix elements of the position operator in the Bloch basis $\{|m\mathbf{k}\rangle\}$ of \hat{H}_0 ,

$$r_{mn\mathbf{k}}^z = \langle m\mathbf{k} | \hat{r}_z | n\mathbf{k} \rangle. \quad (4)$$

Because z is non-periodic, these matrix elements are gauge independent and free of the Berry-phase ambiguity that affects in-plane components [48]. Using a localized-orbital representation $|\alpha\mathbf{k}\rangle = \sum_{\mathbf{R}} e^{i\mathbf{k}\cdot\mathbf{R}} |\alpha\mathbf{R}\rangle$, with orbital index α and lattice vector \mathbf{R} , the position matrix elements can be decomposed into on-site and intersite contributions. For the z component one can write

$$r_{mn\mathbf{k}}^z = r_{nn\mathbf{k}}^{z,\text{on}} + r_{mn\mathbf{k}}^{z,\text{inter}}, \quad (5)$$

where the on-site part depends only on the z -coordinates of the orbital centers $d_z^{(\alpha)}$,

$$r_{mn\mathbf{k}}^{z,\text{on}} = \sum_{\alpha} c_{\alpha\mathbf{k}}^{(m)*} c_{\alpha\mathbf{k}}^{(n)} d_z^{(\alpha)}, \quad (6)$$

and $r_{mn\mathbf{k}}^{z,\text{inter}}$ collects all remaining intersite terms involving overlaps $\langle \alpha\mathbf{0} | \hat{r}_z | \alpha'\mathbf{R} \rangle$ with either $\mathbf{R} \neq \mathbf{0}$ or $\alpha \neq \alpha'$. In minimal tight-binding models built from point-like planar orbitals, $r_{mn\mathbf{k}}^{z,\text{inter}}$ is often neglected and $d_z^{(\alpha)}$ may be identical for all orbitals in a given layer, so the static field effectively enters only as a layer-resolved on-site potential. In contrast, Wannier Hamiltonians constructed from *ab initio* calculations naturally generate finite intersite dipole matrix elements [48, 49, 51, 56], allowing the static field to modify both orbital hybridization and band dispersion. This distinction is crucial in planar systems or in centrosymmetric multilayers, where purely on-site models can artificially suppress the coupling to the static field.

B. Second-order dc response

The dc photocurrent to second-order in the optical field can be written as

$$j_a(0) = \sum_{bc} \sigma_{abc}^{(2)}(\omega; E_{\text{DC}}) E_b^{(\text{ac})} E_c^{(\text{ac})}, \quad (7)$$

where $\sigma_{abc}^{(2)}(\omega; 0)$ reduces to the usual second-order conductivity containing shift and injection contributions [53]. In our approach, the dependence on the static field is fully contained in the eigenvalues and eigenstates of the field-dressed Hamiltonian,

$$\hat{H}_0^{(\text{DC})} |n\mathbf{k}\rangle = \varepsilon_{n\mathbf{k}} |n\mathbf{k}\rangle. \quad (8)$$

We obtain these eigenstates by expanding either in the Bloch basis $\{|m\mathbf{k}\rangle\}$ or, equivalently, in the Wannier basis $\{|\alpha\mathbf{k}\rangle\}$. In the Bloch representation, Eq. (8) becomes

$$\sum_n \left[\varepsilon_{n\mathbf{k}}^{(0)} \delta_{mn} - eE_{\text{DC}} r_{mn\mathbf{k}}^z \right] c_{n\mathbf{k}}^{(n)} = \varepsilon_{n\mathbf{k}} c_{m\mathbf{k}}^{(n)}, \quad (9)$$

with $r_{mn\mathbf{k}}^z$ as in Eq. (5). The resulting eigenvalues $\varepsilon_{n\mathbf{k}}$ and eigenvectors $|n\mathbf{k}\rangle$ define a new equilibrium ground state in the presence of the static field, on top of which the optical perturbation is treated to first order.

Using the field-dressed eigenstates in the length-gauge formalism of Sipe and Shkrebta [53], the shift contribution to the BPVE can be expressed as

$$\begin{aligned} \sigma_{abc}^{(\text{shift})}(\omega; E_{\text{DC}}) &= \\ &- \frac{\pi e^3}{\hbar^2} \sum_{mn} f_{mn} (R_{mn}^{ca} - R_{nm}^{cb}) r_{nm}^b r_{mn}^a \delta(\omega_{nm} - \omega), \end{aligned} \quad (10)$$

where $f_{mn} = f_m - f_n$ is the occupation difference, r_{mn}^b are dipole matrix elements in the field-dressed basis, $\omega_{nm} = (\varepsilon_n - \varepsilon_m)/\hbar$, and $R_{nm}^{a,b}$ is the shift vector. All these quantities depend implicitly on E_{DC} through Eq. (8). For time-reversal-symmetric systems and linearly polarized light, the injection contribution vanishes and the real part of $\sigma^{(2)}$ coincides with the shift conductivity [53]; this is the quantity we focus on throughout.

C. Connection with third-order response

For our purposes it is sufficient to retain only those contributions to the dc current that depend on the optical field. In frequency space, one can write schematically

$$\begin{aligned} J_{\text{DC}}^a &= \sigma_{abc}^{(2)}(0; \omega, -\omega) E_b(\omega) E_c(-\omega) \\ &+ \sigma_{abcd}^{(3)}(0; \omega, -\omega, 0) E_b(\omega) E_c(-\omega) E_d(0) \\ &+ \dots, \end{aligned} \quad (11)$$

where $E_d(0)$ denotes the static field component and $\sigma_{abcd}^{(3)}(0; \omega, -\omega, 0)$ encodes the static field-induced shift, injection, and jerk currents [32, 33]. In our scheme, the second-order photoconductivity $\sigma_{abc}^{(2)}(\omega; E_{\text{DC}})$ is computed non-perturbatively with respect to E_{DC} via the field-dressed Hamiltonian. Assuming that $\sigma_{abc}^{(2)}(\omega; E_{\text{DC}})$ is smooth around $E_{\text{DC}} = 0$, we can write a Taylor expansion

$$\sigma_{abc}^{(2)}(\omega; E_{\text{DC}}) = \sigma_{abc}^{(2,0)}(\omega) + E_{\text{DC}} \sigma_{abc}^{(2,1)}(\omega) + \mathcal{O}(E_{\text{DC}}^2), \quad (12)$$

with

$$\sigma_{abc}^{(2,1)}(\omega) = \frac{\partial}{\partial E_{\text{DC}}} \sigma_{abc}^{(2)}(\omega; E_{\text{DC}}) \Big|_{E_{\text{DC}}=0}. \quad (13)$$

Since in our setup the static field points along z , this first-order coefficient is directly related to the mixed third-order tensor via

$$\sigma_{abcz}^{(3)}(0; \omega, -\omega, 0) = \sigma_{abc}^{(2,1)}(\omega), \quad (14)$$

so that the linear-in-field part of our non-perturbative $\sigma_{abc}^{(2)}(\omega; E_{\text{DC}})$ reproduces the components $\sigma_{abcz}^{(3)}$ of the fourth-rank tensor derived in Refs. [32, 33]. Because the static field is applied strictly along z , our calculations probe this particular tensor slice, with $a, b, c \in \{x, y, z\}$ and fixed static field index z .

In centrosymmetric crystals, $\sigma_{abc}^{(2,0)}(\omega) = 0$ by symmetry, so the leading nonzero shift current at small E_{DC} is linear in the static field and entirely governed by $\sigma_{abcz}^{(3)}(0; \omega, -\omega, 0)$. This behavior will become clear in our results below, where $\sigma_{abc}^{(2)}(\omega; E_{\text{DC}})$ is strictly zero at $E_{\text{DC}} = 0$ and grows linearly at weak fields. At larger E_{DC} , deviations from linearity signal the onset of higher-order terms in Eq. (12), which are fully captured by the field-dressed Hamiltonian and are responsible for the saturation and eventual suppression of the shift current observed in our numerical results.

D. Symmetry Analysis

Before presenting the numerical results it is useful to summarize how a perpendicular static field modifies the point-group symmetry of the systems considered. The symmetry fixes which components of the second-order conductivity tensor $\sigma_{abc}^{(2)}$ [57] can be nonzero and explains the different qualitative responses of monolayer, 2H bilayer, and 3R bilayer MoS₂.

1. Monolayer

At zero static field the monolayer belongs to the D_{3h} point group. The horizontal mirror σ_h forbids all tensor components that contain an odd number of z indices, so the allowed shift conductivity is restricted to in-plane components. A perpendicular static field E_{DC} removes σ_h and all operations that reverse the z axis, such as the C_2' rotations and the S_3 rotoinversions. The remaining operations are the threefold rotation C_3 and the three vertical mirrors σ_v , which form the C_{3v} point group, with non-zero components arranged as in Eq. 15. Under this reduced symmetry all components permitted by C_{3v} are allowed, including those that involve z [57]:

$$\begin{aligned} \sigma^{x;xx} &= -\sigma^{x;yy} = -\sigma^{y;yx}, \\ \sigma^{z;zz}, \\ \sigma^{x;xz} &= \sigma^{y;yz}, \\ \sigma^{z;xx} &= \sigma^{z;yy}. \end{aligned} \quad (15)$$

In practice, the new components remain small because the monolayer is thin along z , and the field can only induce a limited out-of-plane charge displacement.

2. 2H bilayer (AA' stacking)

The 2H bilayer belongs to the centrosymmetric D_{3d} point group at zero field. Inversion symmetry enforces $\sigma_{abc}^{(2)} = 0$ for all tensor components in equilibrium. When a perpendicular static field is applied, inversion and the rotoinversion operations are broken, while the threefold axis and the three vertical mirrors are preserved. The symmetry is therefore reduced from D_{3d} to C_{3v} , which is the same point group as the field-dressed monolayer. In this situation all C_{3v} -allowed tensor components become finite. The difference with the monolayer is not the existence of additional symmetry channels but the way the field polarizes the system. In the bilayer, the two layers are related by inversion at zero field and are separated along z . Once the inversion is broken, the field induces opposite charge displacements in the two layers and generates a sizable shift conductivity, both in in-plane components and in mixed components that involve z . This explains why the field-induced response of the 2H bilayer is much stronger than the small corrections that appear in the monolayer.

3. 3R bilayer (AB stacking)

The 3R bilayer lacks inversion and also lacks the horizontal mirror already at zero static field, so it belongs to the C_{3v} point group in equilibrium. As a result, the shift current is nonzero even without external static field and the nonvanishing components follow the C_{3v} pattern. A perpendicular static field keeps the point group unchanged, so the set of symmetry-allowed tensor components is the same. What changes is the built-in layer asymmetry. The stacking already produces an intrinsic potential difference between the two layers. Depending on its sign, the external field can either reinforce the built-in polarity or counteract it. These competing contributions allow the shift conductivity to be tuned in opposite directions, and in some cases the effective asymmetry can be significantly reduced. The numerical results in Sec. III show this behavior clearly in components such as $\sigma_{zzz}^{(2)}$. The allowed tensor components take the form

Overall, a perpendicular field brings all three systems into a common C_{3v} framework, each via a distinct symmetry-breaking route. The monolayer starts from D_{3h} and acquires C_{3v} under a static field, which activates additional components that remain relatively small. The 2H bilayer starts from D_{3d} , has no second-order response in the absence of a field, and develops a strong shift conductivity once inversion is broken. The 3R bilayer is already C_{3v} at zero field, and the external static field tunes

an intrinsic shift current by either amplifying or compensating the built-in layer polarity. This unified symmetry picture underlies the distinct field dependences observed in the numerical results.

III. RESULTS

A. MoS₂ Monolayer

As discussed in the symmetry analysis, the monolayer acquires C_{3v} symmetry under a perpendicular static field, which activates tensor components containing out-of-plane indices. However, the effect is expected to be weak because the monolayer is thin along z and the induced charge redistribution is limited. Here, and throughout the cases presented in this section, our analysis therefore focuses on photon energies near the bandgap, where the response is well converged and of primary physical interest, while higher-energy features may be affected by the finite k mesh.

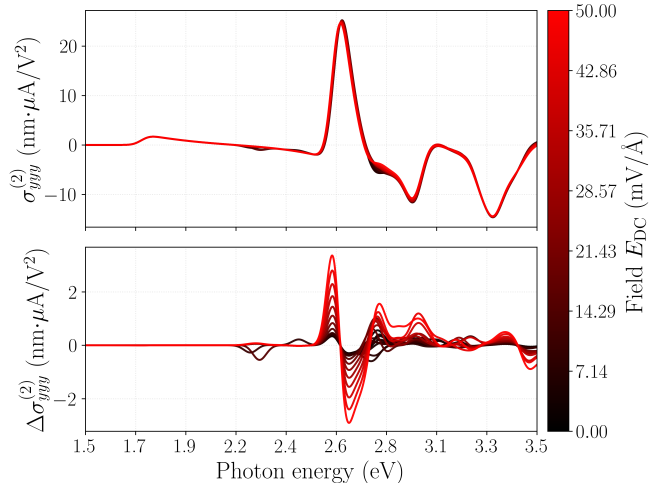


FIG. 1. second-order conductivity $\sigma_{yy}^{(2)}(\omega; E_{DC})$ of monolayer MoS₂ under static out-of-plane fields up to 0.050 mV/Å. The top panel shows the full spectrum and the bottom panel shows the differential response $\Delta\sigma_{yy}^{(2)}(\omega; E_{DC})$. Field-induced changes remain weak, on the order of 2.5 nm·μA/V².

To quantify the effect of the static field we examine the differential response $\Delta\sigma(\omega; E_{DC}) = \sigma(\omega; E_{DC}) - \sigma(\omega; 0)$. In-plane components such as $\sigma_{yy}^{(2)}$ are already allowed at zero field and remain essentially unchanged, as shown in Fig. 1. This behavior agrees with SHG measurements where the monolayer signal varies weakly under gating while bilayers show a strong dependence [26]. This is also consistent with DFT studies showing that the monolayer bandgap is nearly insensitive to a perpendicular static field [58].

The situation changes for tensor elements involving out-of-plane indices. As shown in Fig. 2, the perpendicular field activates components such as $\sigma_{zyy}^{(2)}$, $\sigma_{yyz}^{(2)}$,

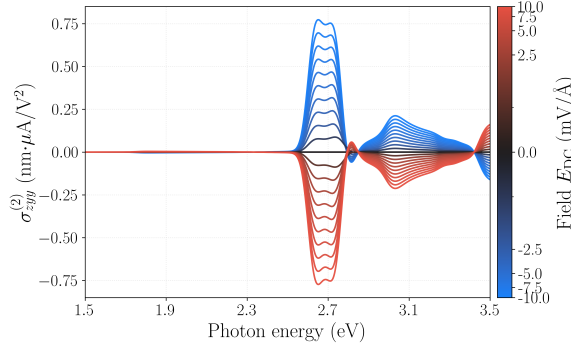


FIG. 2. Representative out-of-plane component of the shift conductivity tensor in monolayer MoS₂ under a perpendicular static field.

and $\sigma_{zxx}^{(2)}$. These components display an antisymmetric dependence on E_{DC} , consistent with the odd character of the perturbation $-eE_{DC}\hat{r}_z$. In the small-field regime with $|E_{DC}| \lesssim 5$ meV/Å, the behavior is linear and follows the Taylor expansion discussed in Sec. II. Beyond this regime, at larger fields with $|E_{DC}| \gtrsim 50$ meV/Å, the curves saturate, which reflects the limited out-of-plane polarizability and the nonlinear reshaping of the band structure. Among the newly activated components, $\sigma_{zxx}^{(2)}$ and $\sigma_{zyy}^{(2)}$ exhibit the largest variations. Their magnitudes exceed those of $\sigma_{zzz}^{(2)}$ and $\sigma_{yyz}^{(2)}$ by well over an order of magnitude, highlighting a strong coupling between in-plane optical excitation and out-of-plane charge redistribution.

B. 2H-MoS₂ Bilayer

As summarized in the symmetry analysis, the 2H (AA') bilayer belongs to the centrosymmetric D_{3d} point group at zero field and therefore has vanishing second-order conductivity in equilibrium. A perpendicular static field E_{DC} breaks inversion and lowers the symmetry to C_{3v} , which activates all tensor components allowed by this point group. In contrast to the monolayer, where the field mainly generates small out-of-plane components, the 2H bilayer develops sizeable in-plane and mixed components once inversion is broken, leading to a strong field-induced shift current.

Figure 3 shows the evolution of $\sigma_{yyy}^{(2)}(\omega; E_{DC})$ and $\sigma_{zyy}^{(2)}(\omega; E_{DC})$ under finite field. At $E_{DC} = 0$ the conductivity vanishes identically for all tensor components and a finite response appears immediately once inversion is broken. The overall response increases with the static field. Among the components that involve an out-of-plane index, the mixed component $\sigma_{yyz}^{(2)}$ dominates, being significantly larger than $\sigma_{zzy}^{(2)}$ and $\sigma_{zzz}^{(2)}$. A more detailed review of the low-field regime and the saturation onset is given in Fig. 4, discussed below.

The origin of this saturation can be understood by ex-

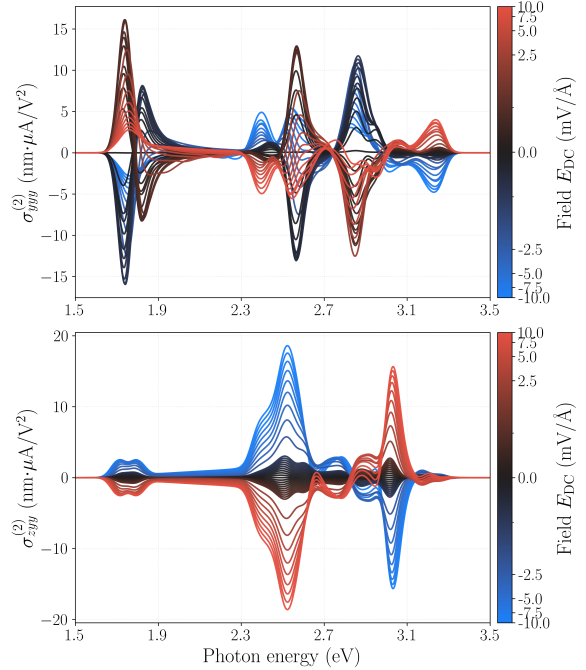


FIG. 3. In-plane (top) and out-of-plane (bottom) shift conductivity for 2H-MoS₂ under a perpendicular static field E_{DC} .

amining the three ingredients that enter the shift conductivity, namely the shift vector \mathbf{R} , the oscillator strength $\mathcal{A} = v_{cv}^a v_{vc}^b$, and the set of resonant \mathbf{k} points selected by the condition $E_{cv}(\mathbf{k}) = \hbar\omega$. At small fields the shift vector grows steadily with E_{DC} and follows the initial increase of $\sigma^{(2)}$. At the same time the oscillator strength decreases because the field polarizes the charge density along z , which reduces the overlap between conduction and valence states. The band structure is also modified by the field. As the gap narrows, the resonant \mathbf{k} points that satisfy $E_{cv} = \hbar\omega$ move away from the original valley and form a ring where \mathcal{A} is intrinsically weaker. The apparent reduction in \mathcal{A} is therefore dominated by the migration of resonant momenta rather than by a direct suppression of the velocity matrix elements. The growth of \mathbf{R} and the weakening of \mathcal{A} compete. At sufficiently large E_{DC} the latter effect dominates, so the conductivity stops increasing and eventually decreases, which marks the onset of the saturation regime.

Among the newly activated components, $\sigma_{zxx}^{(2)} = \sigma_{zyy}^{(2)}$ shows the largest amplitude. Its magnitude is roughly one order of magnitude larger than $\sigma_{zzz}^{(2)}$ and several times larger than $\sigma_{yyz}^{(2)}$. This again indicates a strong coupling between in-plane optical excitation and out-of-plane charge redistribution, in line with the monolayer results but with a much stronger absolute response.

The static field also renormalizes the electronic structure. The direct band gap decreases approximately linearly with the applied field, with a slope of about -3.23 eV/(V/Å), in agreement with photoluminescence experiments and simulations [58–60]. This redshift pro-

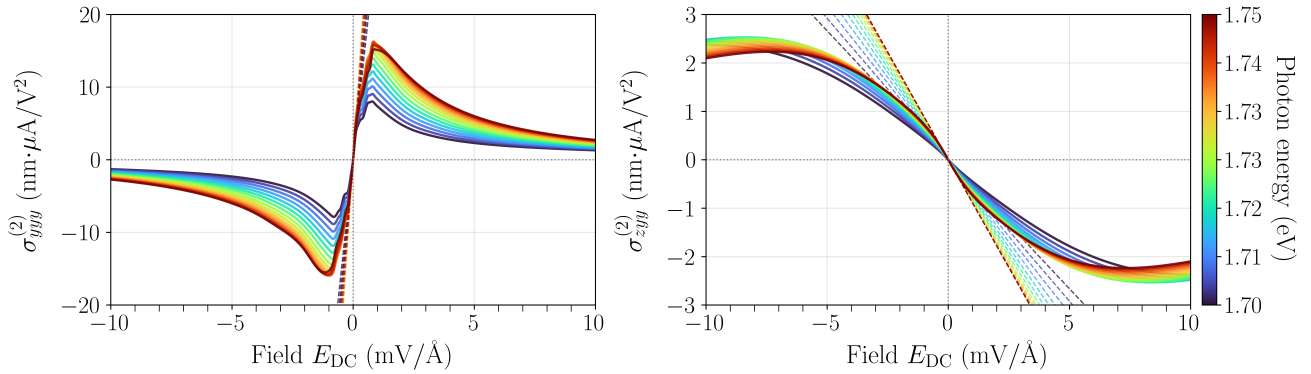


FIG. 4. Field dependence of the second-order conductivity for 2H-MoS₂. Left panels: $\sigma_{yy}^{(2)}(\omega; E_{DC})$ and its derivative with respect to E_{DC} for several photon energies near the band edge. Right panels: corresponding results for $\sigma_{zyy}^{(2)}(\omega; E_{DC})$. The dashed lines show the linear behavior extracted from the derivative at $E_{DC} = 0$, which corresponds to the mixed third-order conductivity $\sigma_{abcz}^{(3)}(0; \omega, -\omega, 0)$ through Eq. (12). The linear regime around zero field verifies the Taylor expansion, while deviations at larger fields reveal the onset of higher-order field dependence.

duces a clear drift of the optical peaks with increasing E_{DC} . The most intense peaks in $\sigma^{(2)}$ appear well above the absorption edge, around 1.3 to $1.5E_g$, in agreement with GW–BSE studies of the linear optical spectrum of MoS₂ [61]. Those works showed that the absorption in this range is dominated by higher-lying excitations with significant contributions from states away from the K valleys and with orbital characters beyond the simple d_{z^2} conduction-band edge. The independent-particle approximation does not capture exciton binding energies or any sub-gap excitations, but the enhanced response is consistent with the presence of such strongly allowed transitions.

The detailed behavior at low and intermediate fields is shown in Fig. 4. For weak static fields, $\sigma_{yy}^{(2)}$ grows linearly with the static field up to $|E_{DC}| \lesssim 1$ mV/Å, whereas components that contain out-of-plane indices remain linear up to approximately $|E_{DC}| \lesssim 7.5$ mV/Å. For larger fields the response saturates. The in-plane components exhibit a sharper inflection, whereas the out-of-plane ones saturate more gradually. The saturation field also depends on photon energy, so different frequencies show different onset values.

In this linear regime, the response satisfies $\sigma_{yy}^{(2)}(\omega; E_{DC}) \approx \sigma_{zyyz}^{(3)} E_{DC}$ as expected from the Taylor expansion discussed in Sec. II. The derivative with respect to E_{DC} is nearly constant in this range, which confirms the direct link between the induced second-order response and the third-order conductivity. At larger fields the derivative develops strong oscillations, indicating the breakdown of the first-order Taylor expansion and the growing importance of higher-order terms as hoppings and intersite dipoles depend nonlinearly on E_{DC} .

It is instructive to compare the centrosymmetric 2H bilayer with the monolayer, as shown in Figure 5. The monolayer response is almost insensitive to E_{DC} , while in the bilayer the same static field activates a strong

and tunable $\sigma^{(2)}$. An analogous distinction between monolayer and bilayer responses is seen in electric-field-controlled SHG experiments on bilayer MoS₂ [26], where the monolayer exhibits little variation with applied field while the bilayer displays a strong linear increase. In nonlinear optics it is common to write an effective susceptibility $\chi_{\text{eff}}^{(2)} \propto \chi^{(3)} E_{DC}$, which leads to an SHG intensity that scales as $I_{2\omega} \propto E_{DC}^2$. In the present case an analogous mechanism appears in the photoconductivity. The field-dressed Hamiltonian produces an effective $\sigma_{\text{eff}}^{(2)} \propto E_{DC}$, which yields a dc current that is linear in the external static field and quadratic in the optical field. Field-induced shift current and EFISH therefore emerge

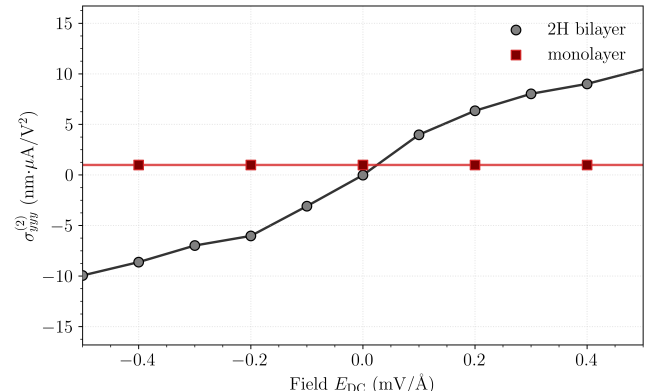


FIG. 5. Comparison between the field-induced second-order conductivity of centrosymmetric 2H (AA') bilayer MoS₂ (black circles) and the intrinsic monolayer response (red squares) at $\hbar\omega \approx E_g$. The bilayer exhibits a strong (essentially) linear dependence on E_{DC} , while the monolayer remains nearly constant. The sign reversal for opposite field polarities reflects the antisymmetric character of the field-induced shift current, which vanishes in the centrosymmetric limit.

from the same symmetry-breaking process [28, 62].

C. 3R-MoS₂ Bilayer

The 3R-stacked (AB) bilayer MoS₂ belongs to the non-centrosymmetric C_{3v} point group, which is the same symmetry that the monolayer and the 2H bilayer acquire only after inversion is broken. As a result, the shift current is already finite at zero static field, with nonzero tensor components given by Eq. 15. A perpendicular static field E_{DC} does not change the point group, but it modifies the potential difference between the layers and the degree of interlayer hybridization. In this case the field acts as a tuning parameter for the second-order response rather than as a symmetry-enabling perturbation.

For the in-plane response, the effect of E_{DC} is similar to the monolayer, since components such as $\sigma_{yyy}^{(2)}$ remain nearly unchanged as the field increases. The main difference appears in tensor elements that contain out-of-plane indices. These components are highly sensitive to the magnitude and sign of E_{DC} and display a clear anti-symmetric dependence, which is consistent with the odd character of the perturbation $-eE_{DC}\hat{r}_z$. A representative case is shown in Fig. 6 for the $\sigma_{zzz}^{(2)}$ component.

Unlike the 2H bilayer, where all components vanish in the centrosymmetric limit and grow from zero once inversion is broken, the 3R stacking already supports intrinsic shift conductivity in every symmetry-allowed component. When the external field is applied, the perturbation $-eE_{DC}\hat{r}_z$ can either reinforce or oppose the built-in polarity of the stacking. One field orientation enhances the intrinsic asymmetry and increases the shift conductivity, while the opposite polarity partially compensates the internal potential difference. At a particular field strength the two contributions nearly cancel and the effective layer asymmetry is strongly reduced. In this situation the shift current is suppressed and the response mimics a temporary restoration of a mirror-like character across the xy plane.

This compensation effect has no analogue in the monolayer or in the 2H bilayer. In the monolayer, in-plane components are almost insensitive to E_{DC} and out-of-plane components only appear once the field breaks the horizontal mirror. In the 2H stacking, the static field activates a response that is strictly zero at $E_{DC} = 0$ and initially grows linearly with the field. The 3R structure therefore represents an intermediate case, where an external static field can either amplify or quench an already finite shift current. The $\sigma_{zzz}^{(2)}$ component, which does not couple to in-plane optical fields, provides a particularly clear example of this behavior and is shown in Fig. 6.

Similar field-polarity compensation effects have been reported in ferroelectric photovoltaic devices and gate-tunable van der Waals heterostructures, where external fields or gate voltages can enhance, suppress, or even reverse photocurrents by competing with built-in fields [63, 64]. However, to the best of our knowledge, an

analogous compensation mechanism has not been explicitly demonstrated for shift-current responses in non-ferroelectric 3R-stacked transition-metal dichalcogenides.

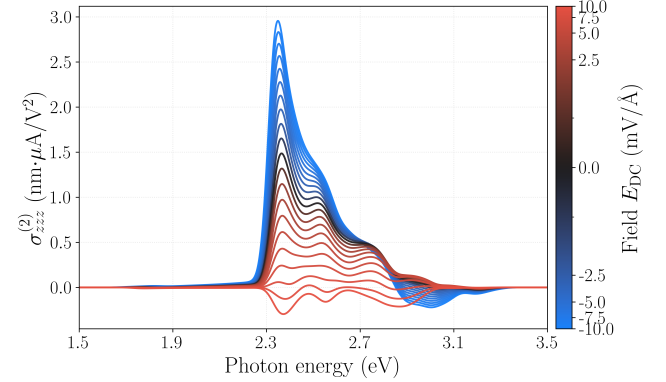


FIG. 6. Field dependence of $\sigma_{zzz}^{(2)}(\omega; E_{DC})$ in 3R-stacked MoS₂. Positive and negative static fields modulate the intrinsic response in opposite directions, and a strong suppression appears when the external field compensates the built-in polarity of the stacking.

IV. CONCLUSIONS

We have shown that a static out-of-plane electric field provides an effective way to enable and tune shift-current responses in two-dimensional materials. Using a combined DFT-Wannier-XATU.Optix workflow [65], we demonstrated how the field breaks inversion in the 2H bilayer and activates a strong second-order response that grows linearly at small static fields and saturates at larger fields. The monolayer and 3R bilayer remain in the same C_{3v} class under the field, but their responses differ markedly because the field either generates new out-of-plane components in the monolayer or tunes an already finite shift current in the polar 3R stacking.

The onset and saturation of the field-induced response occur well below the dielectric breakdown limit. The field strengths explored here extend from 1 mV/Å to 10 mV/Å to illustrate the full evolution of the response, although the relevant behavior appears within experimentally accessible values below 0.1 mV/Å. These trends provide a microscopic basis for the field control of photovoltaic effects in devices and broaden the range of nonlinear optical phenomena available in centrosymmetric layered materials.

ACKNOWLEDGMENTS

J.J. Esteve-Paredes thanks Daniel J. Passos for helpful discussions. This work has been funded by the Spanish Ministry of Science, Innovation and Universities & the State Research Agency (MCIU/AEI/FEDER,UE)

through grants TED2021-131323BI00 and PID2022-141712NB-C21, the "María de Maeztu" Programme for Units of Excellence in R&D (CEX2023-001316-M), the Comunidad de Madrid within the Recovery, Transformation and Resilience Plan, and by NextGenerationEU programme from the European Union through the project "Disruptive 2D materials" (MAD2D-CMUAM7) and the Generalitat Valenciana through the Program Prometeo (2021/017). We also acknowledge computer resources and assistance provided by Centro de Computación Científica de la Universidad Autónoma de Madrid and RES resources (FI-2025-1-12, FI-2024-3-0010, FI-2024-2-0016, FI-2024-1-0038, FI-2023-3-0049, and FI-2023-2-0013). Guilherme I. Janone and Wendel S. Paz acknowledge financial support from the Brazilian funding agencies FAPES (1044/2022, 1081/2022 – P:2022-8L35F, and 875/2023 – P:2023-V36VC) and CNPq (under grants 444450/2024-6, 305227/2024-6, and 442781/2023-7). They are also grateful for the computational resources provided by the Sci-Com Lab/UFES. Guilherme J. Inacio expresses his gratitude to Darian Leucian Pele for fruitful discussions.

Appendix A COMPUTATIONAL METHODS

A Electronic structure

The electronic structure of MoS_2 was obtained from density functional theory calculations performed with the QUANTUM ESPRESSO package [66]. Exchange-correlation effects were described within the generalized gradient approximation using the Perdew-Burke-Ernzerhof functional [67]. Core-valence interactions were treated with KJPAW pseudopotentials. A plane-wave cutoff of 50 Ry for the wavefunctions and 310 Ry for the charge density was used together with an $18 \times 18 \times 1$ Monkhorst-Pack grid. Atomic positions were relaxed

until residual forces were smaller than 10^{-3} (a.u) and the change in total energy was smaller than 10^{-4} (a.u). A vacuum spacing of 20 Å was included to avoid spurious interactions between periodic replicas, and vander-Waals dispersion forces were included through D3 Grimme corrections [68].

B Wannier Hamiltonian

The low-energy Hamiltonian was constructed using the WANNIER90 code [50]. Closest Wannier Functions (CWFs) [51, 56] were employed in place of maximally localized Wannier functions to preserve atomic character and ensure gauge continuity in the presence of the static field. Mo s , p and d orbitals, and S s and p orbitals were used as projectors, and the disentanglement window was selected with a Fermi-Dirac smearing ranging from $T_0 = 10^{-6}$ K to $T_1 = 5$ K. No maximal localization procedure was applied. The resulting Hamiltonian reproduces the DFT band structure near the Fermi level and provides well-behaved intersite position-matrix elements $r_{\alpha\alpha'k}^{(z)}$ needed for the static field coupling.

C Optical and shift-conductivity calculations

The linear and nonlinear conductivities were obtained within the independent-particle approximation using the open-source XATU.OPTIX package [54, 55, 65]. XATU.OPTIX evaluates the second-order tensor $\sigma_{abc}^{(2)}(0; \omega, -\omega)$ from the velocity and dipole matrix elements of the Wannier Hamiltonian. All spectra were computed using a Lorentzian broadening of $\hbar\eta = 0.030$ eV and sampling over 161 neighbouring cells in the Brillouin zone. Excitonic effects were not included so that the influence of the static field on the single-particle band structure can be isolated.

[1] S. Wu, L. Mao, A. M. Jones, W. Yao, C. Zhang, and X. Xu, "Quantum-Enhanced Tunable Second-Order Optical Nonlinearity in Bilayer Graphene," *Nano Letters*, vol. 12, pp. 2032–2036, Apr. 2012. Publisher: American Chemical Society.

[2] J. E. Spanier, V. M. Fridkin, A. M. Rappe, A. R. Akbashev, A. Polemi, Y. Qi, Z. Gu, S. M. Young, C. J. Hawley, D. Imbrenda, *et al.*, "Power conversion efficiency exceeding the shockley–queisser limit in a ferroelectric insulator," *Nature Photonics*, vol. 10, no. 9, pp. 611–616, 2016.

[3] G. B. Osterhoudt, L. K. Diebel, M. J. Gray, X. Yang, J. Stanco, X. Huang, B. Shen, N. Ni, P. J. Moll, Y. Ran, *et al.*, "Colossal mid-infrared bulk photovoltaic effect in a type-I Weyl semimetal," *Nature materials*, vol. 18, no. 5, pp. 471–475, 2019.

[4] T. C. Berkelbach, M. S. Hybertsen, and D. R. Reichman, "Theory of neutral and charged excitons in monolayer transition metal dichalcogenides," *Physical Review B—Condensed Matter and Materials Physics*, vol. 88, no. 4, p. 045318, 2013.

[5] M. O. Sauer, A. Taghizadeh, U. Petralanda, M. Ovesen, K. S. Thygesen, T. Olsen, H. Cornean, and T. G. Pedersen, "Shift current photovoltaic efficiency of 2D materials," *npj Computational Materials*, vol. 9, p. 35, Mar. 2023.

[6] Z. Dai and A. M. Rappe, "Recent progress in the theory of bulk photovoltaic effect," *Chemical Physics Reviews*, vol. 4, p. 011303, Jan. 2023.

[7] S. M. Young and A. M. Rappe, "First principles calculation of the shift current photovoltaic effect in ferroelectrics," *Physical review letters*, vol. 109, no. 11, p. 116601, 2012.

[8] Y.-H. Chan, D. Y. Qiu, F. H. da Jornada, and S. G. Louie, "Giant exciton-enhanced shift currents and direct current conduction with subbandgap photo excitations produced by many-electron interactions," *Proceedings of the National Academy of Sciences*, vol. 118, p. e1906938118, June 2021. Publisher: Proceedings of the National Academy of Sciences.

[9] R. W. Boyd, A. L. Gaeta, and E. Giese, "Nonlinear optics," in *Springer Handbook of Atomic, Molecular, and Optical Physics*, pp. 1097–1110, Springer, 2008.

[10] Á. R. Puente-Uriona, S. S. Tsirkin, I. Souza, and J. Ibañez-Azpiroz, "Ab initio study of the nonlinear optical properties and dc photocurrent of the Weyl semimetal TaIrTe₄," *Physical Review B*, vol. 107, p. 205204, May 2023. Publisher: American Physical Society.

[11] J. C. G. Henriques, B. Amorim, R. M. Ribeiro, and N. M. R. Peres, "Excitonic response of AA' and AB stacked hBN bilayers," *Physical Review B*, vol. 105, p. 115421, Mar. 2022. Publisher: American Physical Society.

[12] J. Ruan, Y.-H. Chan, and S. G. Louie, "Exciton Enhanced Nonlinear Optical Responses in Monolayer h-BN and MoS₂: Insight from First-Principles Exciton-State Coupling Formalism and Calculations," *Nano Letters*, vol. 24, pp. 15533–15539, Dec. 2024. Publisher: American Chemical Society.

[13] A. Taghizadeh and T. G. Pedersen, "Nonlinear optical selection rules of excitons in monolayer transition metal dichalcogenides," *Physical Review B*, vol. 99, p. 235433, June 2019.

[14] M. F. C. M. Quintela, N. M. R. Peres, and T. G. Pedersen, "Tunable nonlinear excitonic optical response in biased bilayer graphene," *Physical Review B*, vol. 110, p. 085433, Aug. 2024.

[15] Y. Xiong, L.-k. Shi, and J. C. Song, "Atomic configuration controlled photocurrent in van der waals homostructures," *2D Materials*, vol. 8, no. 3, p. 035008, 2021.

[16] Y. Wei, W. Li, Y. Jiang, and J. Cheng, "Electric field induced injection and shift currents in zigzag graphene nanoribbons," *Physical Review B*, vol. 104, no. 11, p. 115402, 2021.

[17] S. J. Brun and T. G. Pedersen, "Intense and tunable second-harmonic generation in biased bilayer graphene," *Physical Review B*, vol. 91, no. 20, p. 205405, 2015.

[18] H. Yu, D. Talukdar, W. Xu, J. B. Khurgin, and Q. Xiong, "Charge-Induced Second-Harmonic Generation in Bilayer WSe₂," *Nano Letters*, vol. 15, pp. 5653–5657, Aug. 2015. Publisher: American Chemical Society.

[19] M. Berciano, G. Marcaud, P. Damas, X. Le Roux, P. Crozat, C. Alonso Ramos, D. Pérez Galacho, D. Benedikovic, D. Marris-Morini, E. Cassan, and L. Vivien, "Fast linear electro-optic effect in a centrosymmetric semiconductor," *Communications Physics*, vol. 1, p. 64, Oct. 2018. Publisher: Nature Publishing Group.

[20] T.-J. Shao, Y. Xu, X.-H. Huang, and X.-B. Bian, "Strain effects on high-order harmonic generation in solids," *Physical Review A*, vol. 99, no. 1, p. 013432, 2019.

[21] L. Mennel, M. Paur, and T. Mueller, "Second harmonic generation in strained transition metal dichalcogenide monolayers: MoS₂, MoSe₂, WS₂, and WSe₂," *APL Photonics*, vol. 4, p. 034404, Dec. 2018.

[22] I. Maity, A. A. Mostofi, and J. Lischner, "Atomistic theory of twist-angle dependent intralayer and interlayer exciton properties in twisted bilayer materials," *npj 2D Materials and Applications*, vol. 9, p. 20, Mar. 2025. Publisher: Nature Publishing Group.

[23] Y. Gao, Y. Zhang, and D. Xiao, "Tunable layer circular photogalvanic effect in twisted bilayers," *Physical Review Letters*, vol. 124, no. 7, p. 077401, 2020.

[24] Y. Shan, Y. Li, D. Huang, Q. Tong, W. Yao, W.-T. Liu, and S. Wu, "Stacking symmetry governed second harmonic generation in graphene trilayers," *Science advances*, vol. 4, no. 6, p. eaat0074, 2018.

[25] Z. Zheng, K. Chang, and J. L. Cheng, "Gate voltage induced injection and shift currents in AA- and AB-stacked bilayer graphene," *Physical Review B*, vol. 108, Dec. 2023. Publisher: American Physical Society (APS).

[26] J. Klein, J. Wierzbowski, A. Steinhoff, M. Florian, M. Rosner, F. Heimbach, K. Muller, F. Jahnke, T. O. Wehling, J. J. Finley, *et al.*, "Electric-field switchable second-harmonic generation in bilayer MoS₂ by inversion symmetry breaking," *Nano letters*, vol. 17, no. 1, pp. 392–398, 2017.

[27] S. Wang, W. Li, C. Deng, Z. Hong, H.-B. Gao, X. Li, Y. Gu, Q. Zheng, Y. Wu, P. G. Evans, J.-F. Li, C.-W. Nan, and Q. Li, "Giant electric field-induced second harmonic generation in polar skyrmions," *Nature Communications*, vol. 15, p. 1374, Feb. 2024. Publisher: Nature Publishing Group.

[28] S. Chen, K. F. Li, G. Li, K. W. Cheah, and S. Zhang, "Gigantic electric-field-induced second harmonic generation from an organic conjugated polymer enhanced by a band-edge effect," *Light: Science & Applications*, vol. 8, p. 17, Jan. 2019. Publisher: Nature Publishing Group.

[29] L. Gu and Y. Zhou, "Nonlinear optics in 2D materials: From classical to quantum," *Applied Physics Reviews*, vol. 12, p. 011335, Mar. 2025.

[30] D. Wickramaratne, L. Weston, and C. G. Van de Walle, "Monolayer to Bulk Properties of Hexagonal Boron Nitride," *The Journal of Physical Chemistry C*, vol. 122, pp. 25524–25529, Nov. 2018. Publisher: American Chemical Society.

[31] Y. Fujimoto and S. Saito, "Band engineering and relative stabilities of hexagonal boron nitride bilayers under biaxial strain," *Physical Review B*, vol. 94, p. 245427, Dec. 2016. Publisher: American Physical Society.

[32] B. M. Fregoso, R. A. Muniz, and J. Sipe, "Jerk Current: A Novel Bulk Photovoltaic Effect," *Physical Review Letters*, vol. 121, p. 176604, Oct. 2018. Publisher: American Physical Society.

[33] B. M. Fregoso, "Bulk photovoltaic effects in the presence of a static electric field," *Physical Review B*, vol. 100, Aug. 2019. Publisher: American Physical Society (APS).

[34] E. V. Castro, K. S. Novoselov, S. V. Morozov, N. M. R. Peres, J. M. B. L. dos Santos, J. Nilsson, F. Guinea, A. K. Geim, and A. H. C. Neto, "Biased Bilayer Graphene: Semiconductor with a Gap Tunable by the Electric Field Effect," *Physical Review Letters*, vol. 99, p. 216802, Nov. 2007. Publisher: American Physical Society.

[35] F. Zaabar, F. Mahrouche, S. Mahtout, F. Rabilloud, and K. Rezouali, "Effects of an external electric field on the electronic properties and optical excitations of germanane and silicane monolayers," *Journal of Physics: Condensed Matter*, vol. 35, p. 175502, Mar. 2023. Publisher: IOP Publishing.

[36] N. D. Drummond, V. Zólyomi, and V. I. Fal'ko, "Electrically tunable band gap in silicene," *Physical Review B*, vol. 85, p. 075423, Feb. 2012. Publisher: American

Physical Society.

[37] A. Chakrabarty and S. Datta, "Fate of Wannier-Stark localization and skin effect in periodically driven non-Hermitian quasiperiodic lattices," *Physical Review B*, vol. 111, p. 174202, May 2025. Publisher: American Physical Society.

[38] C. De Beule, S. Gassner, S. Talkington, and E. Mele, "Floquet-bloch theory for nonperturbative response to a static drive," *Physical Review B*, vol. 109, no. 23, p. 235421, 2024.

[39] W. J. Yu, Y. Liu, H. Zhou, A. Yin, Z. Li, Y. Huang, and X. Duan, "Highly efficient gate-tunable photocurrent generation in vertical heterostructures of layered materials," *Nature Nanotechnology*, vol. 8, pp. 952–958, Dec. 2013.

[40] O. Slobodyan, J. Flicker, J. Dickerson, J. Shoemaker, A. Binder, T. Smith, S. Goodnick, R. Kaplar, and M. Hollis, "Analysis of the dependence of critical electric field on semiconductor bandgap," *Journal of Materials Research*, vol. 37, no. 4, pp. 849–865, 2022.

[41] Z. Wang, T. Zhang, M. Ding, B. Dong, Y. Li, M. Chen, X. Li, J. Huang, H. Wang, X. Zhao, Y. Li, D. Li, C. Jia, L. Sun, H. Guo, Y. Ye, D. Sun, Y. Chen, T. Yang, J. Zhang, S. Ono, Z. Han, and Z. Zhang, "Electric-field control of magnetism in a few-layered van der Waals ferromagnetic semiconductor," *Nature Nanotechnology*, vol. 13, pp. 554–559, July 2018. Publisher: Nature Publishing Group.

[42] S. Kovalchuk, K. Greben, A. M. Kumar, S. Pessel, J. Soyka, Q. Cao, K. Watanabe, T. Taniguchi, D. Christiansen, M. Selig, A. Knorr, S. Eigler, and K. I. Bolotin, "Revealing hidden interlayer excitons in 2D bilayers via hybrid molecular gating," *Nature Communications*, vol. 16, p. 9893, Nov. 2025. Publisher: Nature Publishing Group.

[43] B. I. Weinrib, Y.-L. Hsieh, S. Kovalchuk, J. N. Kirchhoff, K. Greben, and K. I. Bolotin, "Generating intense electric fields in 2D materials by dual ionic gating," *Nature Communications*, vol. 13, p. 6601, Nov. 2022. Publisher: Nature Publishing Group.

[44] C.-E. Fillion, J. Fischer, R. Kumar, A. Fassatoui, S. Pizzini, L. Ranno, D. Ourdani, M. Belmeguenai, Y. Roussigné, S.-M. Chérif, *et al.*, "Gate-controlled skyrmion and domain wall chirality," *Nature Communications*, vol. 13, no. 1, p. 5257, 2022.

[45] T. Hiraoka, S. Nestler, W. Zhang, S. Rossel, H. A. Hafez, S. Fabretti, H. Schlörb, A. Thomas, and D. Turchinovich, "Terahertz field effect in a two-dimensional semiconductor," *Nature Communications*, vol. 16, p. 5235, June 2025. Publisher: Nature Publishing Group.

[46] A. Rashidi, S. Ahadi, S. Munyan, W. J. Mitchell, and S. Stemmer, "Tuning Displacement Fields in a Two-Dimensional Topological Insulator Using Nanopatterned Gates," *Nano Letters*, vol. 24, pp. 7366–7372, June 2024. Publisher: American Chemical Society.

[47] A. J. Green, K. D. Chabak, E. R. Heller, R. C. Fitch, M. Baldini, A. Fiedler, K. Irmischer, G. Wagner, Z. Galazka, S. E. Tetlak, *et al.*, "3.8-MV/cm breakdown strength of MOVPE-grown Sn-doped beta-Ga₂O₃ MOSFETs," *IEEE Electron Device Letters*, vol. 37, no. 7, pp. 902–905, 2016.

[48] R. Resta, "Quantum-mechanical position operator in extended systems," *Physical Review Letters*, vol. 80, no. 9, p. 1800, 1998.

[49] J. J. Esteve-Paredes and J. J. Palacios, "A comprehensive study of the velocity, momentum and position matrix elements for Bloch states: Application to a local orbital basis," *SciPost Physics Core*, vol. 6, p. 002, Jan. 2023.

[50] A. A. Mostofi, J. R. Yates, G. Pizzi, Y.-S. Lee, I. Souza, D. Vanderbilt, and N. Marzari, "An updated version of wannier90: A tool for obtaining maximally-localised wannier functions," *Computer Physics Communications*, vol. 185, no. 8, pp. 2309–2310, 2014.

[51] T. Ozaki, "Closest wannier functions to a given set of localized orbitals," *Physical Review B*, vol. 110, no. 12, p. 125115, 2024.

[52] C. Aversa and J. E. Sipe, "Nonlinear optical susceptibilities of semiconductors: Results with a length-gauge analysis," *Physical Review B*, vol. 52, pp. 14636–14645, Nov. 1995. Publisher: American Physical Society.

[53] J. E. Sipe and A. I. Shkrebtii, "Second-order optical response in semiconductors," *Phys. Rev. B*, vol. 61, p. 5337, 2000.

[54] J. J. Esteve-Paredes, M. A. García-Blázquez, A. J. Uría-Álvarez, M. Camarasa-Gómez, and J. J. Palacios, "Excitons in nonlinear optical responses: shift current in MoS₂ and GeS monolayers," *npj Computational Materials*, vol. 11, p. 13, Jan. 2025.

[55] A. J. Uría-Álvarez, J. J. Esteve-Paredes, M. García-Blázquez, and J. J. Palacios, "Efficient computation of optical excitations in two-dimensional materials with the xatu code," *Computer Physics Communications*, vol. 295, p. 109001, 2024.

[56] R. Oiwa, A. Inda, S. Hayami, T. Nomoto, R. Arita, and H. Kusunose, "Symmetry-adapted closest Wannier modeling based on complete multipole basis set," *Physical Review B*, vol. 112, p. 035116, July 2025. Publisher: American Physical Society.

[57] M. A. García-Blázquez, J. J. Esteve-Paredes, A. J. Uría-Álvarez, and J. J. Palacios, "Shift Current with Gaussian Basis Sets and General Prescription for Maximally Symmetric Summations in the Irreducible Brillouin Zone," *Journal of Chemical Theory and Computation*, vol. 19, pp. 9416–9434, Dec. 2023.

[58] Q. Liu, L. Li, Y. Li, Z. Gao, Z. Chen, and J. Lu, "Tuning Electronic Structure of Bilayer MoS₂ by Vertical Electric Field: A First-Principles Investigation," *The Journal of Physical Chemistry C*, vol. 116, pp. 21556–21562, Oct. 2012.

[59] T. Chu, H. Ilatikhameneh, G. Klimeck, R. Rahman, and Z. Chen, "Electrically Tunable Bandgaps in Bilayer MoS₂," *Nano Letters*, vol. 15, pp. 8000–8007, Dec. 2015. Publisher: American Chemical Society.

[60] X. Sun, Y. Chen, D. Zhao, T. Taniguchi, K. Watanabe, J. Wang, and J. Xue, "Measuring Band Modulation of MoS₂ with Ferroelectric Gates," *Nano Letters*, vol. 23, pp. 2114–2120, Mar. 2023. Publisher: American Chemical Society.

[61] D. Y. Qiu, F. H. da Jornada, and S. G. Louie, "Optical Spectrum of MoS₂: Many-Body Effects and Diversity of Exciton States," *Physical Review Letters*, vol. 111, p. 216805, Nov. 2013. Publisher: American Physical Society.

[62] H. Fan, A. Proskurin, M. Song, Y. Kivshar, and A. Bogdanov, "Electric-Field-Induced Second-Harmonic Generation," July 2025. arXiv:2507.09306 [physics].

[63] Y. Li, J. Fu, X. Mao, C. Chen, H. Liu, M. Gong, and H. Zeng, "Enhanced bulk photovoltaic effect in two-

dimensional ferroelectric cuinp₂s₆,” *Nature communications*, vol. 12, no. 1, p. 5896, 2021.

[64] Y. Bai, W. Hao, Y. Wang, J. Tian, C. Wang, Y. Lei, Y. Yang, X. Yao, Q. Liu, C. Li, M. Gu, and J. Wang, “Anomalous photocurrent reversal for the same polarization direction in van der waals ferroelectric cuinp₂s₆,” *PRX Energy*, vol. 3, no. 2, p. 023004, 2024.

[65] A. J. Uría-Álvarez, J. J. Esteve-Paredes, and M. A. García-Blázquez, “Xatu.”

[66] P. Giannozzi, S. Baroni, N. Bonini, M. Calandra, R. Car, C. Cavazzoni, D. Ceresoli, G. L. Chiarotti, M. Cococcioni, I. Dabo, *et al.*, “Quantum espresso: a modular and open-source software project for quantum simulations of materials,” *Journal of physics: Condensed matter*, vol. 21, no. 39, p. 395502, 2009.

[67] J. P. Perdew, K. Burke, and M. Ernzerhof, “Generalized gradient approximation made simple,” *Phys. Rev. Lett.*, vol. 77, p. 3865, 1996.

[68] S. Grimme, “Semiempirical GGA-type density functional constructed with a long-range dispersion correction,” *Journal of computational chemistry*, vol. 27, no. 15, pp. 1787–1799, 2006.